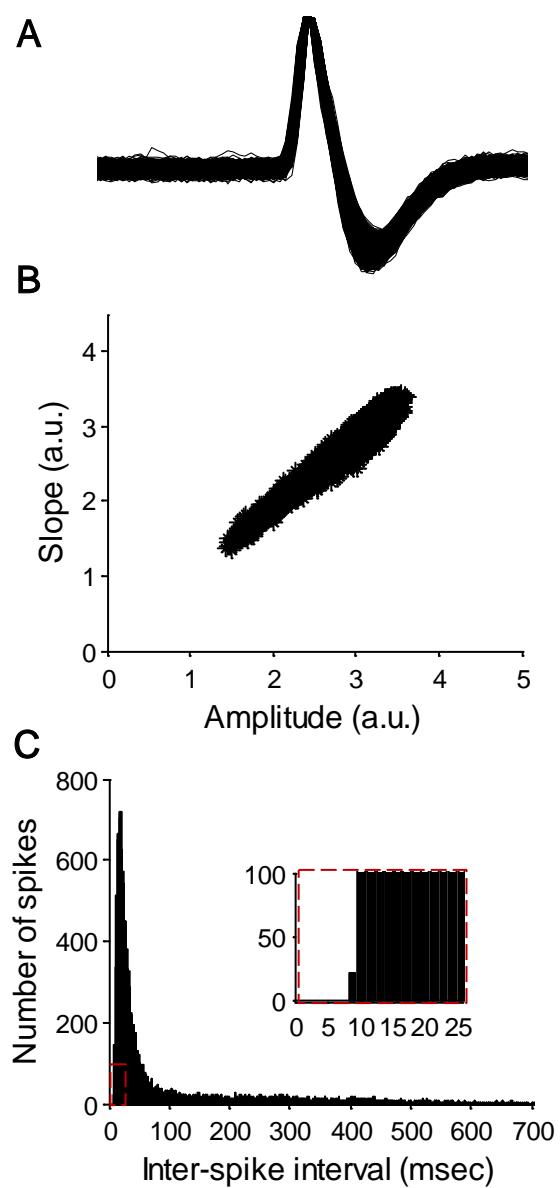


Neuron, Volume 81

Supplemental Information

Odor Processing by Adult-Born Neurons

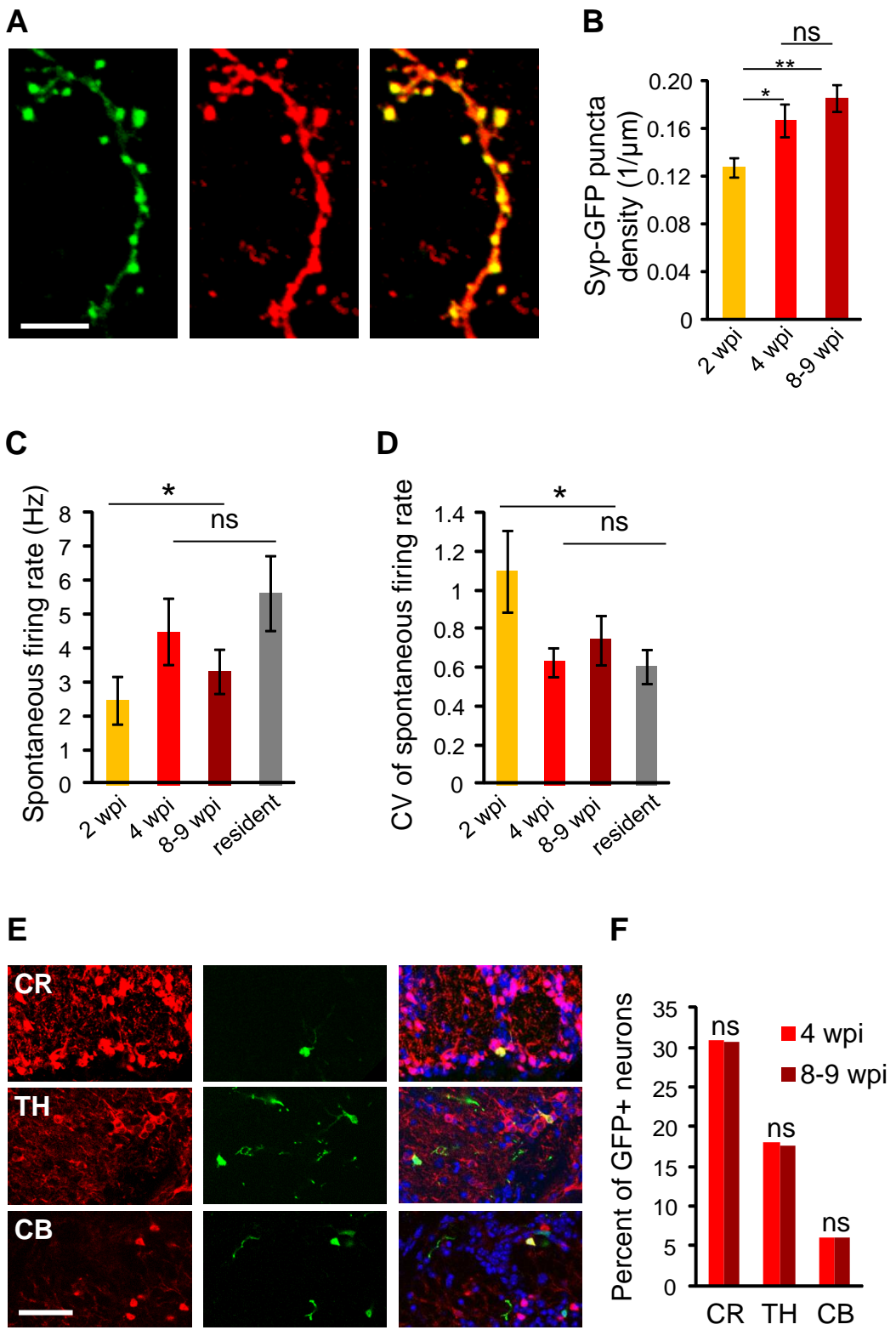
Yoav Livneh, Yoav Adam, and Adi Mizrahi



Supplemental Figure S1, related to Figure 1: Verification of Single Neuron Recordings.

Example of the procedure for verification of single neuron recordings (see Experimental Procedures for further details).

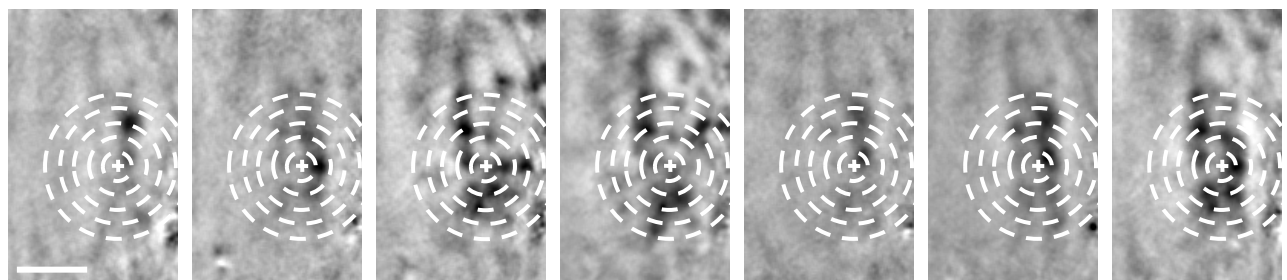
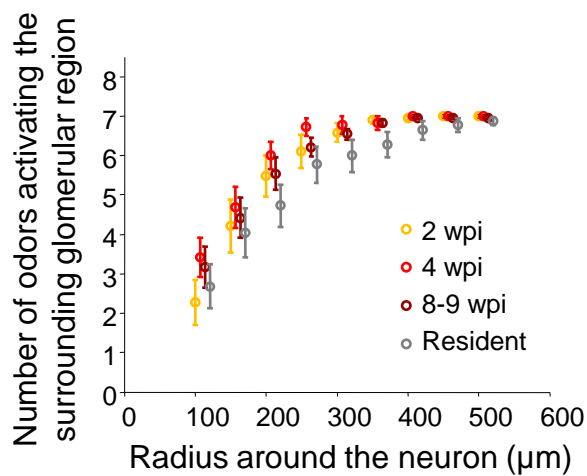
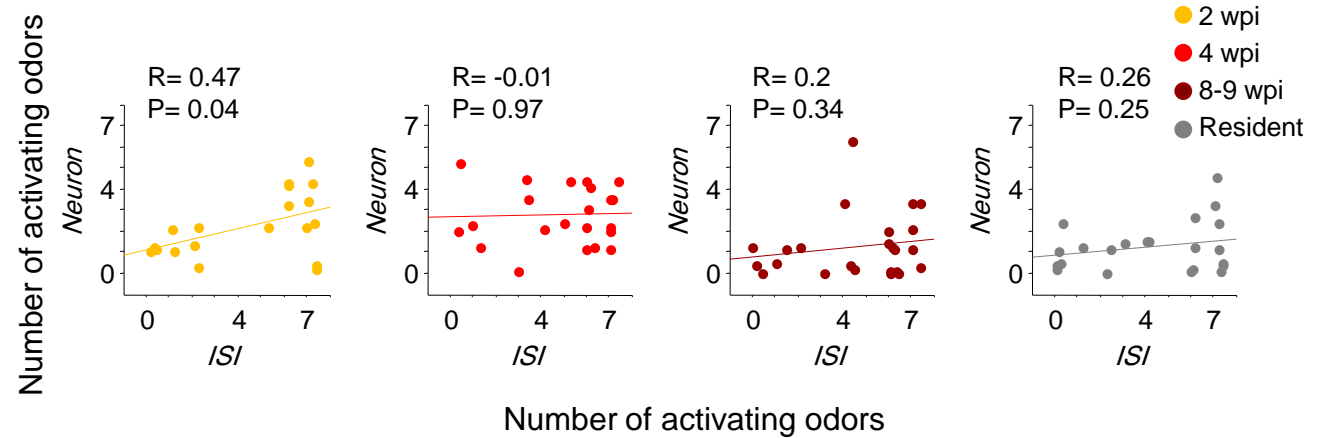
- A. Overlay of all spikes of the cell from Fig. 2B, showing similar waveforms.
- B. Analysis of the relation between spike amplitude and slope for all spikes from the same cell in A, showing a single cluster.
- C. Analysis of inter-spike interval of all spikes from the same cell in A.



Supplemental Figure S2

Supplemental Figure S2, related to Figure 3: Development of Putative Presynapses, Spontaneous Spiking Activity and PGN subtypes.

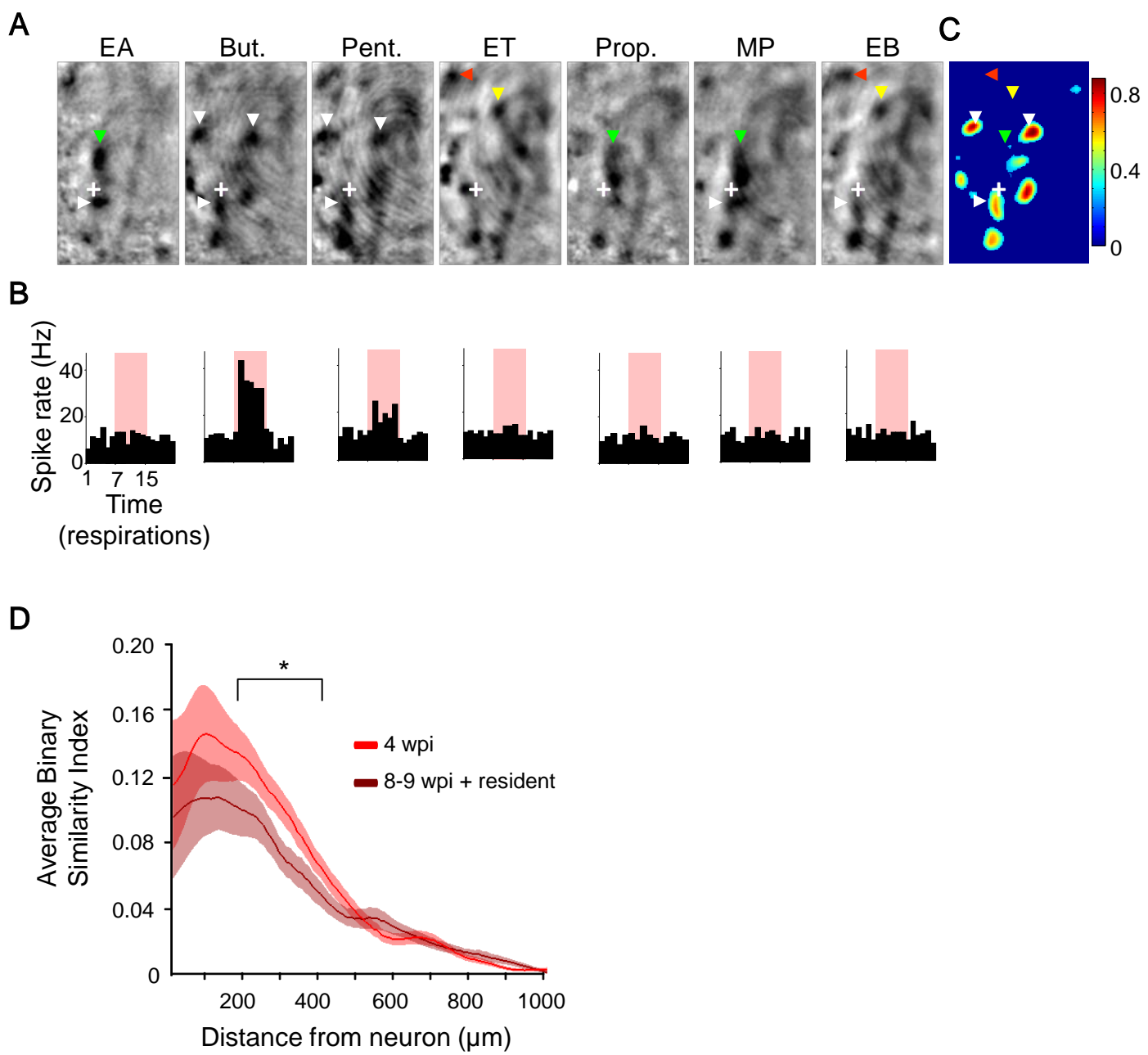
- A. Examples of a dendritic branch from an adult-born PGN expressing Syp-GFP (left, green), amplified by an anti-GFP antibody (middle, red) and a merged image (right). Scale bar: 10 μ m.
- B. Quantitative comparison of Syp-GFP puncta density between the different groups. All values are mean \pm s.e.m. * p <0.027, ** p <0.002, ns: not significant, Mann-Whitney test. 2 wpi: n=15 neurons from 4 mice; 4 wpi: n=11 neurons from 3 mice; 8-9 wpi: n=11 neurons from 4 mice.
- C. Spontaneous spike rate in the different experimental groups.
- D. Coefficient of variation (CV) of spontaneous spike rate in the different experimental groups. 2 wpi: n=19 neurons from 6 mice; 4 wpi: n=22 neurons from 11 mice; 8-9 wpi: n= 24 neurons from 9 mice; resident: n= 22 neurons from 16 mice. All values are mean \pm s.e.m. * p <0.03, ns: not significant, Mann-Whitney test.
- E. Single optical plane confocal micrographs showing examples of adult-born PGNs expressing calretinin (CR, top), tyrosine hydroxylase (TH, middle) and calbindin (CB, bottom). Left: immuno-labeled markers (red). Middle: adult-born neurons expressing GFP (green). Right: merge of the green and red channels, also with DAPI (blue). Note that neurons co-expressing GFP and CR/TH/CB appear yellow in the merged images.
- F. Quantification of the percent of GFP-labeled adult-born neurons also expressing the different markers at 4wpi and 8-9 wpi. There was no significant difference between these age groups for all 3 markers (p >0.9 for all comparisons, chi-square test). 4 wpi- CR: 43/139, TH: 25/139, CB: 10/165; 8-9 wpi- CR: 52/170, TH: 30/170, CB: 10/168. N=3 mice for each neuronal age group. Scale bar: 50 μ m, ns: not significant

A**B****C**

Supplemental Figure S3

Supplemental Figure S3, related to Figures 3 & 5: No Spatial Functional Sampling Bias.

- A.** Example ISI maps for all 7 odors. The location of the neuron, recorded in the same OB, is marked with a cross. Dashed circles show radii around the neuron (100–500 μ m). Scale bar: 0.5 mm.
- B.** Quantification of the number of odors activating the region around each neuron with increasing radii during development. There was no significant difference between the groups at all radii ($p>0.05$, Mann-Whitney test).
- C.** Pearson correlation between the number of odors activating each neuron and the glomerular region around it (radius of 150 μ m) for the different groups. There was no significant correlation in all groups except 2 wpi. Similar results were obtained for 200–250 μ m.
- 2 wpi: n=19 neurons from 6 mice; 4 wpi: n=22 neurons from 11 mice; 8–9 wpi: n= 24 neurons from 9 mice; resident: n= 22 neurons from 16 mice. All values are mean \pm s.e.m.



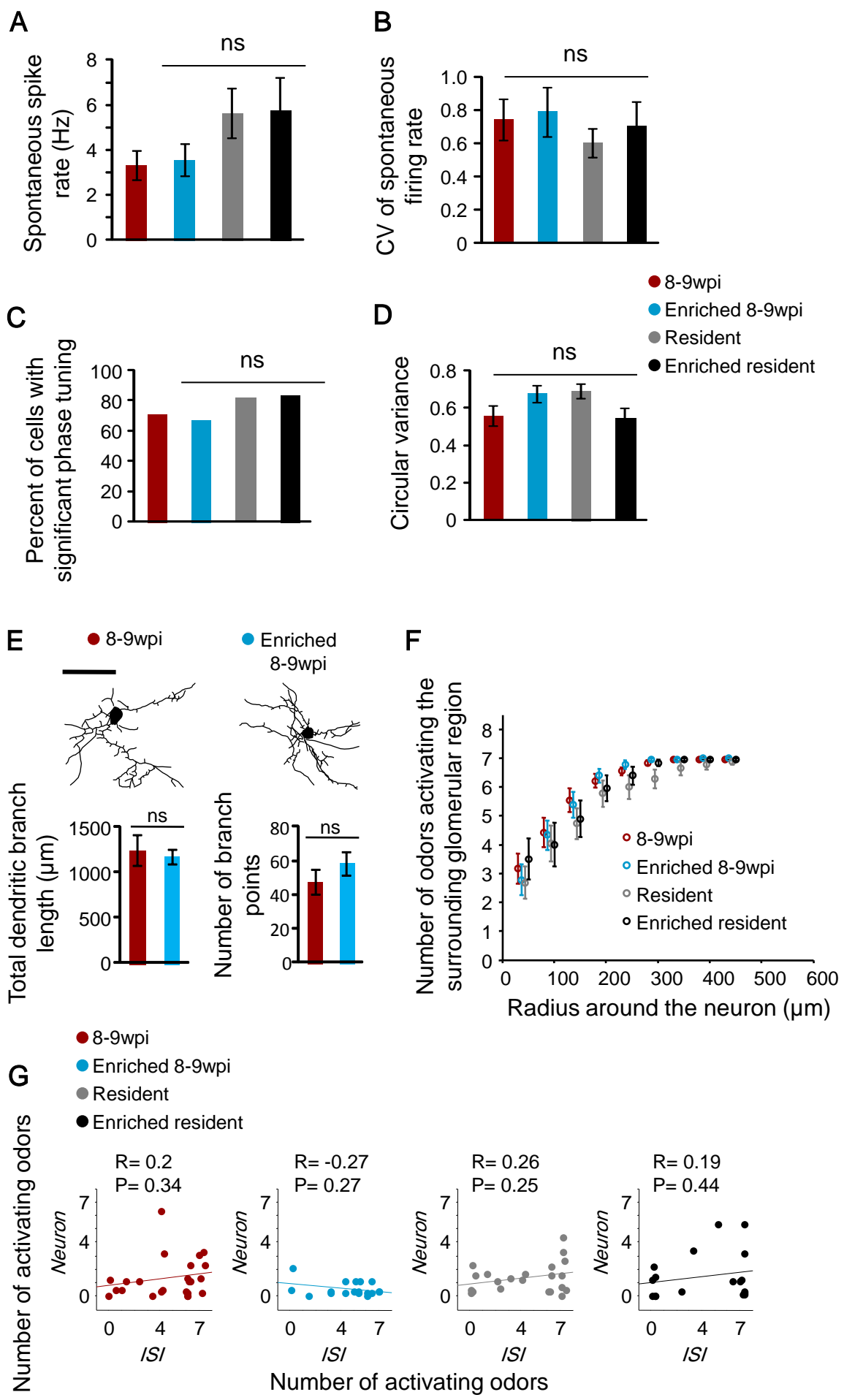
Supplemental Figure S4, related to Figure 5: A-C: Construction of an ISI-Electrophysiology Correlation Map for a Single Neuron. D: Alternative Quantification Using a Binary Similarity Index.

A. ISI maps of the 7 odors. Crosses mark the location of the recorded neuron. White arrowheads point to glomerular foci that appear in the correlation map in 'C'. These glomeruli are candidates to drive the spiking responses of this neuron. Green, red and yellow arrowheads point to glomerular foci that do not appear in the correlation map in 'C'. These glomeruli are not expected to drive any responses in this particular neuron.

B. PSTHs of the neuron's responses to the 7 odors. Pink: 2 sec odor stimulation period.

C. ISI-electrophysiology correlation map, constructed from the ISI maps (A) and neuronal responses (B), after thresholding. Arrowheads are the same as in 'A'. See Experimental Procedures for further details.

D. Alternative quantification of ISI-electrophysiology correlation maps using a binary similarity index. Average pixel similarity index values as a function of the distance from the neuron. All values are mean \pm s.e.m. * $p < 0.04$, ns: not significant, Mann-Whitney test. 4 wpi: n=21 neurons from 11 mice; 8-9 wpi: n= 13 neurons from 6 mice; resident: n= 13 neurons from 12 mice. See Supplemental Experimental Procedures for further details.



Supplemental Figure S5

Supplemental Figure S5, related to Figure 6: A-D: Sensory Experience Does Not Affect Spontaneous Spiking Activity. E: Sensory Experience Does Not Affect Dendritic Morphology. F-G: Verification that there was No Spatial Sampling Bias in the Enrichment Experiment.

A. Spontaneous spike rate in the different experimental groups.

B. Coefficient of variation (CV) of spontaneous spike rate the different experimental groups.

C. Percent of significantly phase tuned cells in the different groups.

D. Circular variance of respiration phase tuning in the different groups.

Enriched 8-9 wpi: n= 18 neurons from 8 mice; Enriched resident: n= 18 neurons from 10 mice. All values are mean \pm s.e.m. ns: not significant, Mann-Whitney test.

E. Top: examples of projections of the 3D reconstructions of 8-9 wpi and enriched 8-9 wpi adult-born neurons. Scale bar: 50 μ m. Bottom: quantitative morphometric analysis of dendritic structure: total dendritic branch length (left), number of branch points per neuron (right). All values are mean \pm s.e.m, ns: not significant, Mann-Whitney test (p=0.38 and p=0.17). 8-9 wpi: n=7 neurons from 4 mice; enriched 8-9 wpi: n=5 neurons from 4 mice.

F. Quantification of the number of odors activating the region around each neuron with increasing radii in the enrichment experiment (same analysis as Supp. Fig. S3). There was no significant difference between the groups at all radii ($p>0.05$, Mann-Whitney test). 8-9 wpi: n= 24 neurons from 9 mice; resident: n= 22 neurons from 16 mice; Enriched 8-9 wpi: n= 18 neurons from 8 mice; Enriched resident: n= 18 neurons from 10 mice. All values are mean \pm s.e.m.

G. Pearson correlation between the number of odors activating each neuron and the glomerular region around it (radius of 150 μ m) for the different groups. There was no significant correlation in all groups. Similar results were obtained for 200-250 μ m (same analysis as Supp. Fig. S3).

Supplemental Experimental Procedures

Animals

We used C57BL/6 mice (8-13 weeks old at the beginning of the experiment). Animal care and experiments were approved by the Hebrew University Animal Care and Use Committee.

Generally, each mouse underwent 3 surgical procedures: lentivirus injections into the rostral migratory stream, intrinsic signal imaging (2-4 wpi), and two-photon targeted recordings (2-9 wpi). In the case of two-photon targeted recordings at 2 wpi, intrinsic signal imaging was performed 3-5 days before injection.

Lentivirus injections

To label adult-born neurons, we injected a lentivirus encoding either GFP (for targeted recordings) or Syp-GFP (for labeling putative presynapses; Kelsch et al., 2008; Kopel et al., 2012) into the rostral migratory stream (RMS), as described previously (Bardy et al., 2010; Livneh and Mizrahi, 2012; Nissant et al., 2009). To generate recombinant lentiviral vectors we sub-cloned a fusion protein of Synaptophysin and GFP (kind gift of D. Gitler, Ben Gurion University of the Negev, Israel) into a lentivirus transfer plasmid under the control of the EF-1 alpha promoter (FESypGW). In addition, to express GFP we used a transfer plasmid with GFP under the control of the CMV promoter (FCGW). Virus was produced by transfection of human embryonic kidney cells (HEK293) with third-generation lentivirus plasmids using polyethylenimine. The medium was collected after 36 h and again after additional 24h. Virus was concentrated using ultracentrifugation and resuspended in PBS.

Lentivirus injections into the RMS were performed as previously described (Livneh and Mizrahi, 2012). We anesthetized mice using ketamine (100 mg per kg of body weight) and medetomidine (0.83 mg per kg of body weight), with carprofen (4 mg per kg of body weight). We also injected saline subcutaneously to prevent dehydration. Depth of anesthesia was assessed by monitoring the pinch withdrawal reflex. Injections were done stereotactically using pressure (coordinates relative to Bregma: anterior- 3.3 mm, lateral- 0.8 mm, ventral- 2.9 mm). After surgery, mice fully recovered and returned to the animal facility under normal housing conditions until intrinsic signal imaging.

Experimental Groups

We used lentivirus injections to label and birth-date adult-born neurons. We and others have previously verified the extent of “noise” of lentivirus birth-dating (Bardy et al., 2010; Livneh and Mizrahi, 2012; Mizrahi, 2007). Neuronal ages in wpi should therefore be regarded as an approximation.

PGNs are comprised of several molecularly defined subtypes, most with yet unknown specific distinct functions (but see Kiyokage et al., 2010 for an exception). Thus, to verify that the differential response profiles during development are not due to some unexpected differential sampling of different subpopulations, we performed immunohistochemical analysis of the main PGN markers at 4 wpi and 8-9 wpi (Supp. Fig. S2; Bagley et al., 2007; Kosaka and Kosaka, 2007; Parrish-Aungst et al., 2007; Whitman and Greer, 2007a). This analysis showed that these subpopulations are represented similarly in both age groups, consistent with previous studies of adult-born PGNs that used BrdU staining and showed no differential survival of a specific subtype (Bagley et al., 2007; Whitman and Greer, 2007a), and similar to previous reports of BrdU staining, suggesting that lentivirus injections are not biased to a specific subtype (compare Supp. Fig. S2 to Bagley et al., 2007; Whitman and Greer, 2007a). Since subtypes are represented similarly in 4 wpi and 8-9 wpi neurons, and we sampled neurons randomly, there is no expected bias towards a specific subtype at any experimental group. Furthermore, because chemical subtype is correlated with dendritic morphology, at least to a certain extent (see e.g., Kiyokage et al., 2010), the reconstructions of the dendritic morphology of our reconstructed neurons demonstrate that morphological subtype heterogeneity is not a predicting factor for the functional changes we observed at 4 wpi and 8-9 wpi. At both these groups neurons were morphologically heterogeneous to a similar extent (see main text). Lastly, the distinct response profiles of enriched 8-9 wpi neurons were not correlated with any morphological changes (Supp. Fig. S5).

Similarly to previous electrophysiological studies of adult-born neurons, we also used GFP-negative neurons as representative of “resident” (or “pre-existing”) neurons (e.g., Ge et al., 2007; Grubb et al., 2008; Nissant et al., 2009; Saghatelian et al., 2005). This sample was not birth-dated using lentivirus RMS injections. However, at any given time point recently-arrived young adult-born neurons comprise a very small fraction of the overall neuronal population. This has been demonstrated for all adult-born neurons both in the hippocampus and olfactory bulb (e.g., Lagace et al., 2007; Ninkovic et al., 2007). Specifically for adult-born PGNs, we and others have shown that they accumulate at a rate of 2-3% per month

(Mizrahi et al., 2006; Ninkovic et al., 2007). Thus, at 4 weeks post injection (wpi) and 8-9 wpi only ~2-3% and ~4-6% of the PGN population will be younger than our recorded neurons. Consequently, in our GFP-negative dataset (n=22), at least 21/22 neurons are older than our 8-9 wpi neurons.

Intrinsic signal imaging

Intrinsic signal imaging (ISI) of the dorsal surface of the OB was performed using an Imager 3001 (Optical Imaging) *via* thinned bone, as described (Livneh et al., 2009; Livneh and Mizrahi, 2012). Briefly, mice were anesthetized using ketamine (100 mg per kg of body weight) and medetomidine (0.83 mg per kg of body weight), with carprofen (4 mg per kg of body weight). We also injected saline subcutaneously to prevent dehydration. Depth of anesthesia was assessed by monitoring the pinch withdrawal reflex. Additionally, we continuously monitored the animal's rectal temperature and maintained it at $36 \pm 1^\circ\text{C}$. Before each ISI experiment, the surface blood vessel pattern was acquired under green light illumination (546 nm). Light reflectance from the surface of the OB (630 nm wavelength light illumination) was captured using a CCD camera (Dalsa 1M60P). Images were acquired with a spatial resolution of $\sim 10 \mu\text{m}/\text{pixel}$ (full frames were 1024x1024 pixels and binned (3x3) for analysis). After surgery, mice fully recovered and returned to the animal facility under normal housing conditions until two-photon targeted recordings.

Two-photon targeted recordings from adult-born neurons

We anesthetized mice with an intraperitoneal injection of ketamine and medetomidine (100 mg/kg and 0.83 mg/kg, respectively), and a subcutaneous injection of carprofen (4 mg/g). We also injected saline subcutaneously to prevent dehydration. Experiments lasted up to 11 hrs (usually ~ 6 hrs). As such, we assessed the depth of anesthesia by monitoring the pinch withdrawal reflex and added ketamine/medetomidine to maintain it. Additionally, we continuously monitored the animal's rectal temperature and maintained it at $36 \pm 1^\circ\text{C}$. For imaging and recording, we made a small incision in the animal's skin, and glued a 0.1 g custom-made metal bar to the skull with dental cement. We used the bar to connect the animal to a custom-made stage to allow positioning of the animal's head for imaging and recording. We then performed a craniotomy ($\sim 1 \times 2$ mm) over the OB of one hemisphere while taking care to ensure that the dura remained intact. To facilitate imaging and recording, we surrounded the OB with a recording well made of dental cement.

We performed the imaging of the OB using an Ultima two-photon microscope from Prairie Technologies (Middleton, WI), equipped with a 16X water-immersion objective lens (0.8 NA; CF175, Nikon). We delivered two-photon excitation (920 nm) with a DeepSee femtosecond laser (Spectraphysics), and expanded the laser beam to fill the large back aperture of the 16X objective. We acquired images of cell bodies (512 X512 pixels) at 0.33-0.13 $\mu\text{m}/\text{pixel}$ resolution in the xy dimension and at 1 $\mu\text{m}/\text{frame}$ in the z dimension.

We pulled electrodes (5 - 10 $M\Omega$) from filamented, thin-walled, borosilicate glass (outer diameter, 1.5 mm; inner diameter, 1.0 mm; Hilgenberg GmbH, Malsfeld, Germany) on a vertical two-stage puller (PC-12, Narishige, EastMeadow, NY). We filled the electrodes with an internal solution containing (in mM): 125 KMeSO₄, 4 KCl, 10 HEPES, 7 phosphocreatine, 3 MgATP, 0.5 NaGTP, and adjusted the pH to 7.3 with KOH. For electrode visualization we supplemented the internal solution with 50-200 μM Alexafluor 568 (Invitrogen). To minimize pulsations we placed 2% percent low melting agar (type IIIa, Sigma-Aldrich) over the craniotomy .

We acquired all recordings using an intracellular amplifier in current clamp mode (Multiclamp 700B, Molecular Devices), at a sampling rate of 10 kHz (Digidata 1440A, Molecular Devices, Sunnyvale, CA). We filtered all recordings using a 100 Hz high-pass filter.

We obtained targeted cell-attached recordings using two-photon visual guidance (Kitamura et al., 2008; Komai et al., 2006; Margrie et al., 2003). We performed all recordings in the glomerular layer (depth 20-80 μm), and verified for each recorded cell that its cell body was indeed in the glomerular layer by filling it with the electrode dye (see below; e.g., Fig. 1B). We approached the electrode towards the labeled cell while applying positive pressure. When the electrode appeared to be touching the cell surface, as was evident from an increase in electrode resistance, we applied negative pressure (20-40 mbar) to obtain a loose seal. We optically verified successful targeting of GFP-labeled cells by electroporating the red fluorescent dye from the electrode into the cell using current pulses and observing the mixing of the red dye with the GFP fluorophore (e.g., Fig. 1B). For analysis, we included only cells that were distinctly filled during this procedure (>40% increase in the red/green intensity ratio, after background subtraction). For the resident neurons group we collected data in two ways. First we used either "shadow patching" (Kitamura et al., 2008) or "blind" patching in the vicinity of GFP-labeled cells. After the end of the recording, we filled the recorded

neuron's cell body to verify that it was in the glomerular layer (e.g., Fig. 3A). Second, as a result of a failed attempt to record from a GFP-labeled cell, the cell body of a GFP-negative cell (adjacent to the GFP-labeled cell) was filled with the electrode dye, and therefore we assigned it to the resident neurons group.

Odor delivery

To deliver odorants we used a custom-made 7-channel olfactometer. In order to avoid cross-contamination between odorants we used separate tubing for each channel, from the odor vial to the animal's nose. For odor delivery, we switched a N₂ stream into one of the odor vials for the desired duration, while keeping the overall flow constant. To control the odor delivery from the olfactometer we used a custom-written MATLAB program, controlling Master-8 (A.M.P.I, Israel). We used a panel of 7 odorants which are known to activate different and partially overlapping areas in the dorsal part of the OB (ethyl-acetate, butanal, pentanal, ethyl-tiglate, propanal, methyl-propionate and ethyl-butyrate; all obtained from Sigma-Aldrich; see e.g., Fig. 2, Supp. Fig. S3). We first diluted the odorants in mineral oil according to their individual vapor pressures to give a nominal headspace concentration of 1000 ppm. We further diluted the odorants by a N₂ flow of 100 ml/min, mixed with a N₂ flow of 900 ml/min, and an additional O₂ flow of 1000 ml/min. This achieves a final concentration of 50 ppm. The flow of the two N₂ channels was controlled using mass flow controllers (M100B, MKS Instruments, Andover, MA). We presented the odorants for 2 sec, with an inter-stimulus interval of 18 sec between individual odors. We repeated the odor presentation usually 7-10 trials (at least 4 trials) in pseudo-random order.

We monitored the animal's respiration throughout the experiment by a low pressure sensor (1-INCH-D1-4V-MINI, 'All sensors'). We connected the low pressure sensor to a thin stainless steel tubing (OD 0.7 mm) which we placed at the entrance of the animals' contralateral nostril. The information from the pressure sensor was passed to an analogue converter (window discriminator), which we used to identify the inhalation onset during the respiratory cycle. We then used a custom-written MATLAB program to trigger odor delivery at inhalation onset.

Immunohistochemistry and confocal microscopy

To obtain OB slices, we perfused mice transcardially with PBS, followed by 4% formaldehyde and cryoprotected the brain in 30% sucrose overnight. We sectioned OBs coronally on a sliding microtome (30 μ m slices), washed the slices in PBS and then incubated them for 1 hr in a blocking solution (5% normal goat serum and 0.5% Triton-X). We incubated slices overnight at room temperature with primary antibodies diluted in the blocking solution (rabbit anti-GFP, Millipore 1:1000; chicken anti-GFP, Millipore 1:1000; rabbit anti-CR, Swant 1:2000; mouse anti-TH, Immunostar 1:500; mouse anti-CB, Swant 1:1000), washed them in PBS, and then incubated them for 3 hrs at room temperature with secondary antibodies (Jackson ImmunoResearch), diluted 1:500 in the blocking solution (Cy3-conjugated goat anti-rabbit; Cy5-conjugated goat anti-mouse; DyeLight488- conjugated goat anti-chicken). Prior to mounting on microscope slides, we incubated the slices with DAPI (Santa Cruz Biotechnology; 50 μ g/ml) for 5 min and then washed them with PBS. We obtained confocal images using an Olympus FV-1000 confocal microscope, or a Leica SP-5 confocal microscope, using a 40X (1.3 NA) oil objective.

Odor enrichment

Odor-enriched mice were housed in their home cages with an “odor pot” (i.e., tea ball), containing 7 odors (either the ‘internal’ or ‘external’ odors), hanging from the top of the cage following standard odor enrichment procedures (Moreno et al., 2009; Rochefort et al., 2002). This odor pot contained 7 swabs, each soaked with 150 μ l of 50 ppm of one of the 7 odors in our stimulus panel. The odorants were replaced daily, approximately every 24 hrs. The odor pot was present in the cage 2wpi-5wpi.

Intrinsic signal imaging data analysis

We analyzed ISI maps offline, using custom written scripts in Matlab. We obtained the normalized ISI signal by $\Delta R/R = (R_{\text{odor}} - R_{\text{air}})/R_{\text{air}}$; where R_{odor} is the ISI signal during the last 2 sec of the 4 sec odor presentation, and R_{air} is the ISI signal during the 2 sec before odor presentation. ISI maps were the averaged response to the odorant in 4 trials. We filtered the $\Delta R/R$ image to remove contamination from a large-scale hemodynamic signal by subtracting a copy convolved with a Gaussian spatial kernel (STD= 315 μ m). For quantitative analysis, we set the threshold for activation at 1.65 standard deviations above the mean signal. This

image processing yields ISI maps that reflect mostly olfactory receptor neuron input to the OB (Fantana et al., 2008; Gurden et al., 2006; Meister and Bonhoeffer, 2001; Soucy et al., 2009; Uchida and Mainen, 2003; Wachowiak and Cohen, 2003).

We used the surface blood vessel pattern to align intrinsic signal images with two-photon images, as described previously (Livneh et al., 2009; Livneh and Mizrahi, 2012), thereby allowing positioning of each neuron's location on the ISI map. ISI was performed 2-5 weeks before the targeted patch recordings; nevertheless, we have previously verified that ISI maps remain stable for many weeks, even after odor enrichment (Livneh et al., 2009; Livneh and Mizrahi, 2012). In addition, we have previously verified that odor exposure during the ISI session does not affect the development of adult-born neurons (Livneh et al., 2009).

To verify that there was no spatial functional sampling bias in any group, we calculated the number of odors that activated a circular region around each neuron with increasing radii (Supp. Fig. S3). We used the same analysis to verify that responsive neurons were more likely to respond to odors that activated the glomerular region around them ($<150\text{ }\mu\text{m}$), than to odors that activated more distal regions (average number of responses to locally activating odors= 1.6 ± 0.2 ; average number of responses to distally activating odors= 0.8 ± 0.16 ; $p=0.0002$). Furthermore, we tested whether the response profiles of glomeruli, adjacent to the recorded neurons, affect the neuronal response profiles. To this end, we examined the correlation between each neuron's response profile (i.e., number of activating odors) and the surrounding glomerular region's response profile at increasing radii around the neurons (Supp. Fig. S3). There was no significant correlation in 4 wpi and 8-9 wpi neurons at all radii, indicating that this factor is not the source of their differential response profiles. Interestingly, at 2 wpi there was a significant correlation at $150\text{-}250\text{ }\mu\text{m}$, but we did not further explore this as we focused mainly on 4 wpi neurons, which showed the most prominent effects (Fig. 3, 5). We repeated the same analysis for the enrichment experiment, and thus verified that the enriched neurons' different response profiles were not a result of their surrounding glomerular region's response profiles (Supp. Fig. S5).

To obtain correlation maps between each neuron and its ISI map (Fig. 5C-E; Supp. Fig. S3), we calculated the similarity of neuronal response to the ISI signal per pixel. We calculated similarity using the uncentered correlation coefficient, as it is insensitive to the overall intensity of the signals and yields values normalized between 0 and 1. We applied this measure to thresholded ISI maps, and to the absolute value of the average change in neuronal firing rate to odors evoking significant responses. The responses to odors that did not evoke a

significant response were set to 0 (Supp. Fig. S4). Unresponsive neurons were not included in this analysis. For quantification, we pooled together mature neurons (8-9 wpi and resident), thereby balancing the number of responsive neurons between the comparison groups (4 wpi: 21 responsive neurons; 8-9 wpi + resident: 26 responsive neurons). We then performed three independent analyses. First, we quantified the number of correlation “hot spots in” each neuron's correlation map (Fig. 5D). Hot spots were defined as circular regions with correlation values >0.25 and a diameter $>100 \mu\text{m}$. We then compared between the groups (Mann-Whitney Test) at equal sized bins ($150 \mu\text{m}$). Second, we calculated the average correlation at increasing distances from the neurons in $10 \mu\text{m}$ bins, while setting below ISI threshold pixels to zero (Fig. 5E). This analysis precludes possible bias due to the hot-spot identification threshold. Third, we used a binary similarity index as another correlation measure. This index was calculated per pixel such that for every odor, each pixel received 1 point if the pixel ISI signal and neuron both responded to the odor, or 0 points for any other possibility. These points were then added up to yield values between 0 and number of odors the neuron responded to. We then normalized these values by dividing them by the number of odors the neuron responded to, thus eliminating possible bias by the higher responsiveness of the young neurons (Supp. Fig. S4). To construct the average maps (Fig. 5C) we performed an average per pixel, while discarding below ISI threshold pixels from the average, and setting a threshold of a minimum of 4 neurons per pixel for calculation of the average correlation for that pixel. Correlation maps were filtered using a Gaussian filter (STD= $100 \mu\text{m}$). Average maps were used for illustration purposes only and were not used for quantitative comparison.

Electrophysiology data analysis

We used custom-written Matlab programs and the CircStat toolbox (Berens, 2009) to perform electrophysiology data analysis. We extracted spikes recorded in cell-attached mode from voltage traces using thresholding. We verified that traces contained only a single unit by waveform analysis and by inter-spike intervals >3 msec (Supp. Fig. S1). We then assigned spike times to the local peaks of supra-threshold segments and rounded them to the nearest millisecond. We measured respiration cycle times by finding local minima and maxima in the respiration trace.

To assess spontaneous firing rate, we calculated the mean spontaneous firing rate based on the 2 sec period that preceded each stimulus, throughout all trials. Variability of spike rate was measured by calculating the coefficient of variation (i.e., relative standard deviation - STD/mean; Supp. Fig. S2, S5). To assess spontaneous phase tuning, we first assigned each spike its timing in its respiration cycle (0- 2π) during the 2 sec preceding odor stimulation. We then checked whether the cell was significantly phase tuned in the respiration cycle by testing for circular uniformity using the Rayleigh test (Bathellier et al., 2008; Batschelet, 1981), accepting significance at $p<0.05$. We measured circular variance by $1-R$, where R is the resultant length of the average phase tuning vector (Bathellier et al., 2008; Batschelet, 1981). For significantly phase-tuned cells, we also calculated the mean angular direction of the spikes.

We defined odor responses as either a change in spike rate (spike rate response), or a change in the angular distribution of spikes in the respiration cycle (respiration phase tuning responses). We detected spike rate responses by comparing the spike rate between the entire 2 sec odor period and the preceding 2 sec period, or by comparing the 2 sec post-odor period and the pre-odor 2 sec period, or by comparing the spike rate in each respiration during the odor period with the average spike rate per respiration during the 2 sec pre-odor period. We applied the Mann-Whitney test for these comparisons, accepting significance at $p<0.05$, except for the analysis of single respirations, in which case we applied the Bonferroni correction for multiple comparisons. We analyzed phase tuning odor responses only if a cell was significantly tuned before and during the odor presentation. We detected spike phase tuning responses by comparing the distribution of spike phases across all trials before and during odor presentation, using a multi-sample test for equal median direction, accepting significance at $p<0.05$ (Fisher, 1995).

We classified odor rate responses as either excitatory (increase in spike rate) or inhibitory (decrease in spike rate). We considered odor responses as inhibitory only if they were not preceded by an excitatory response, and *vice versa*. We calculated response magnitude as the maximal change in firing rate per respiration across odors. We compared percentages of cells of different categories between groups (e.g., the percent of odor-responsive cells; Fig. 3, 6) by using a test for comparison of the proportions of two binomial variables.

Morphological data analysis

For dendritic morphology analysis, we performed reconstructions strictly from the raw data images, obtained during the targeted recording experiments (Fig. 5). We reconstructed dendritic structure manually from the complete 3D image stacks using Neurolucida (MicrobrightField, Colchester, VT).

To examine the number of putative presynapses of adult-born neurons we expressed a presynaptic marker (synaptophysin) fused with GFP (Syp-GFP) in adult-born neuron (Kelsch et al., 2008; Kopel et al., 2012). This was followed by immunohistochemical amplification and confocal analysis of the distribution of Syp-GFP puncta along the dendrites of adult-born neurons at 2, 4 and 8-9 wpi (Supp. Fig. S2; Kelsch et al., 2008; Kopel et al., 2012). We calculated Syp-GFP puncta density from the 3D reconstructions of arbitrarily chosen neurons. We performed 3D reconstructions manually using Neurolucida (MicrobrightField, Colchester, VT) strictly from the raw data images as we described earlier for PSD95-GFP puncta (Livneh et al., 2009).

Using this approach, we found that the density of Syp-GFP puncta along adult-born neurons' dendrites increased significantly between 2 wpi and 8-9 wpi (Supp. Fig. S2). Similar to the dendritic structure results, the density of Syp-GFP puncta of 4 wpi neurons was significantly higher than that of 2 wpi neurons, but not significantly different than that of 8-9 wpi neurons (Supp. Fig. S2). These results suggest that at 4 wpi, adult-born neurons have a similar potential for presynaptic output as that at 8-9 wpi.

All analyses were performed blind to the experimental condition. Quantitative parameters were compared with the Mann-Whitney test.

Supplemental References

- Bardy, C., Alonso, M., Bouthour, W., and Lledo, P.M. (2010). How, when, and where new inhibitory neurons release neurotransmitters in the adult olfactory bulb. *The Journal of neuroscience : the official journal of the Society for Neuroscience* *30*, 17023-17034.
- Bathellier, B., Buhl, D.L., Accolla, R., and Carleton, A. (2008). Dynamic ensemble odor coding in the mammalian olfactory bulb: sensory information at different timescales. *Neuron* *57*, 586-598.
- Batschelet, E. (1981). Circular Statistics in Biology (London Academic Press).
- Berens, P. (2009). CircStat: A MATLAB Toolbox for Circular Statistics. *Journal of Statistical Software* *31*.
- Fantana, A.L., Soucy, E.R., and Meister, M. (2008). Rat olfactory bulb mitral cells receive sparse glomerular inputs. *Neuron* *59*, 802-814.
- Fisher, N.I. (1995). Statistical Analysis of Circular Data. Revised Edition. (Cambridge University Press).
- Gurden, H., Uchida, N., and Mainen, Z.F. (2006). Sensory-evoked intrinsic optical signals in the olfactory bulb are coupled to glutamate release and uptake. *Neuron* *52*, 335-345.
- Kelsch, W., Lin, C.W., and Lois, C. (2008). Sequential development of synapses in dendritic domains during adult neurogenesis. *Proceedings of the National Academy of Sciences of the United States of America* *105*, 16803-16808.
- Kitamura, K., Judkewitz, B., Kano, M., Denk, W., and Hausser, M. (2008). Targeted patch-clamp recordings and single-cell electroporation of unlabeled neurons *in vivo*. *Nature methods* *5*, 61-67.
- Komai, S., Denk, W., Osten, P., Brecht, M., and Margrie, T.W. (2006). Two-photon targeted patching (TPTP) *in vivo*. *Nature protocols* *1*, 647-652.
- Kopel, H., Schechtman, E., Groysman, M., and Mizrahi, A. (2012). Enhanced synaptic integration of adult-born neurons in the olfactory bulb of lactating mothers. *The Journal of neuroscience : the official journal of the Society for Neuroscience* *32*, 7519-7527.
- Livneh, Y., Feinstein, N., Klein, M., and Mizrahi, A. (2009). Sensory input enhances synaptogenesis of adult-born neurons. *The Journal of neuroscience : the official journal of the Society for Neuroscience* *29*, 86-97.
- Livneh, Y., and Mizrahi, A. (2012). Experience-dependent plasticity of mature adult-born neurons. *Nature neuroscience* *15*, 26-28.
- Margrie, T.W., Meyer, A.H., Caputi, A., Monyer, H., Hasan, M.T., Schaefer, A.T., Denk, W., and Brecht, M. (2003). Targeted whole-cell recordings in the mammalian brain *in vivo*. *Neuron* *39*, 911-918.
- Meister, M., and Bonhoeffer, T. (2001). Tuning and topography in an odor map on the rat olfactory bulb. *The Journal of neuroscience : the official journal of the Society for Neuroscience* *21*, 1351-1360.
- Moreno, M.M., Linster, C., Escanilla, O., Sacquet, J., Didier, A., and Mandairon, N. (2009). Olfactory perceptual learning requires adult neurogenesis. *Proceedings of the National Academy of Sciences of the United States of America* *106*, 17980-17985.
- Nissant, A., Bardy, C., Katagiri, H., Murray, K., and Lledo, P.M. (2009). Adult neurogenesis promotes synaptic plasticity in the olfactory bulb. *Nature neuroscience* *12*, 728-730.
- Rochefort, C., Gheusi, G., Vincent, J.D., and Lledo, P.M. (2002). Enriched odor exposure increases the number of newborn neurons in the adult olfactory bulb and improves odor memory. *The Journal of neuroscience : the official journal of the Society for Neuroscience* *22*, 2679-2689.
- Soucy, E.R., Albeau, D.F., Fantana, A.L., Murthy, V.N., and Meister, M. (2009). Precision and diversity in an odor map on the olfactory bulb. *Nature neuroscience* *12*, 210-220.
- Uchida, N., and Mainen, Z.F. (2003). Speed and accuracy of olfactory discrimination in the rat. *Nature neuroscience* *6*, 1224-1229.
- Wachowiak, M., and Cohen, L.B. (2003). Correspondence between odorant-evoked patterns of receptor neuron input and intrinsic optical signals in the mouse olfactory bulb. *Journal of neurophysiology* *89*, 1623-1639.